

# Realization of optical carpets in the Talbot and Talbot-Lau configurations

William B. Case<sup>1,2</sup>, Mathias Tomandl<sup>1</sup>, Sarayut Deachapunya<sup>1,3</sup> and Markus Arndt<sup>1</sup>

<sup>1</sup>University of Vienna, Faculty of Physics, Boltzmannngasse 5, A-1090 Wien

, <sup>2</sup>Grinnell College, P. O. Box 805, Grinnell, Iowa 50112

<sup>3</sup>Department of Physics, Faculty of Science, Burapha University, Chonburi 20131, Thailand.

[markus.arndt@univie.ac.at](mailto:markus.arndt@univie.ac.at)

**Abstract:** Talbot and Talbot-Lau effects are frequently used in lensless imaging applications with light, ultrasound, x-rays, atoms and molecules – generally in situations where refractive optical elements are non-existent or not suitable. We here show an experimental visualization of the intriguing wave patterns that are associated with near-field interferometry behind a single periodic diffraction grating under plane wave illumination and which are often referred to as *Talbot carpets* or *quantum carpets*. We also show the patterns behind two separated diffraction gratings under nearly-monochromatic but spatially incoherent illumination that illustrate the nature of *Talbot-Lau carpets*.

© 2009 Optical Society of America

**OCIS codes:** (050.1940) Diffraction; (000.2060) Education; (100.3175) Interferometric Imaging;

---

## References and links

1. H. F. Talbot, "Facts Relating to Optical Science," *Philos. Mag.* **9**, 401–407 (1836).
2. E. Lau, "Beugungerscheinungen an Doppelrastern," *Ann. Phys.* **6**, 417 (1948).
3. L. Rayleigh, "On Copying Diffraction-Gratings, and some Phenomena Connected Therewith," *Philos. Mag.* **11**, 196 (1881).
4. W. Montgomery, "Self-imaging objects of infinite aperture," *J. Opt. Soc. Am.* **57**(6), 772–775 (1967).
5. K. Patorski, "Incoherent Superposition of Multiple Self-imaging Lau Effect and Moire Fringe Explanation," *Opt. Acta* **30**, 745–758 (1983).
6. G. J. Swanson and E. N. Leith, "Analysis of the Lau Effect and Generalized Grating Imaging," *J. Opt. Soc. Am. A* **2**, 789–793 (1985).
7. L. Liu, "Talbot and Lau effects on incident beams of arbitrary wavefront, and their use," *Appl. Opt.* **28**(21), 4668–4678 (1989).
8. K. Patorski, "Self-Imaging and its Applications," in *Progress in Optics XXVII*, E. Wolf, ed., (Elsevier Science Publishers B. V., Amsterdam, 1989), pp. 2–108.
9. K. Banaszek, K. Wodkiewicz, and W. P. Schleich, "Fractional Talbot effect in Phase Space: A Compact Summation Formula," *Opt. Express* **2**, 169 – 172 (1998).
10. O. Friesch, W. Schleich, and I. Marzoli, "Quantum carpets woven by Wigner functions," *New J. Phys.* **2**(1), 4 (2000).
11. S. Mirza and C. Shaker, "Surface profiling using phase shifting Talbot interferometric technique," *Optical Engineering* **44**, 013,601 (2004).
12. M. Thakur, C. Tay, and C. Quan, "Surface profiling of a transparent object by use of phase-shifting Talbot interferometry," *Appl. Opt.* **44**(13), 2541–2545 (2005).
13. J. Bhattacharya, "Measurement of the refractive index using the Talbot effect and a moire technique," *Appl. Opt.* **28**(13), 2600–2604 (1989).
14. S. Prakash, S. Singh, and A. Verma, "A low cost technique for automated measurement of focal length using Lau effect combined with Moire readout," *J. Mod. Opt.* **53**(14), 2033–2042 (2006).

15. P. Singh, M. Faridi, and C. Shakher, "Measurement of temperature of an axisymmetric flame using shearing interferometry and Fourier fringe analysis technique," *Opt. Eng.* **43**, 387 (2004).
16. G. Spagnolo, D. Ambrosini, and D. Paoletti, "Displacement measurement using the Talbot effect with a Ronchi grating," *J. Opt. A* **4**(6), 376–380 (2002).
17. F. Huang, N. Zheludev, Y. Chen, and F. de Abajo, "Focusing of light by a nanohole array," *Appl. Phys. Lett.* **90**, 091,119 (2007).
18. M. Dennis, N. Zheludev, and F. García de Abajo, "The plasmon Talbot effect," *Opt. Express* **15**(15), 9692–9700 (2007).
19. P. Cloetens, J. Guigay, C. De Martino, J. Baruchel, and M. Schlenker, "Fractional Talbot imaging of phase gratings with hard x rays," *Opt. Lett.* **22**(14), 1059–1061 (1997).
20. F. Pfeiffer, T. Weitkamp, O. Bunk and C. David, "Phase retrieval and differential phase-contrast imaging with low-brilliance X-ray sources," *Nature* **2**, 258–261 (2006).
21. J. F. Clauser and S. Li, "'Heisenberg Microscope' Decoherence Atom Interferometry," *Phys. Rev. A* **50**, 2430 (1994).
22. M. S. Chapman, C. R. Ekstrom, T. D. Hammond, J. Schmiedmayer, B. E. Tannian, S. Wehinger, and D. E. Pritchard, "Near-Field Imaging of Atom Diffraction Gratings: The Atomic Talbot Effect," *Phys. Rev. A* **51**, R14 (1995).
23. S. Nowak, C. Kurtsiefer, T. Pfau, and C. David, "High-Order Talbot Fringes for Atomic Matter Waves," *Opt. Lett.* **22**, 1430–32 (1997).
24. S. B. Cahn, A. Kumarakrishnan, U. Shim, T. Sleator, P. R. Berman, and B. Dubetsky, "Time-Domain de Broglie Wave Interferometry," *Phys. Rev. Lett.* **79**, 784–787 (1997).
25. L. Deng, E. W. Hagley, J. Wen, M. Trippenbach, Y. Band, P. S. Julienne, J. E. Simsarian, K. Helmerson, S. L. Rolston, and W. D. Phillips, "Four-wave mixing with matter waves," *Nature* **398**(6724), 218 (1999).
26. B. Brezger, L. Hackermüller, S. Uttenthaler, J. Petschinka, M. Arndt, and A. Zeilinger, "Matter-Wave Interferometer for Large Molecules," *Phys. Rev. Lett.* **88**, 100,404 (2002).
27. S. Gerlich, L. Hackermüller, K. Hornberger, A. Stibor, H. Ulbricht, M. Gring, F. Goldfarb, T. Savas, M. Müri, M. Mayor, and M. Arndt, "A Kapitza-Dirac-Talbot-Lau interferometer for highly polarizable molecules," *Nat. Phys.* **3**, 711 – 715 (2007).
28. B. J. McMorran and A. D. Cronin, "An electron Talbot interferometer," *New J. Phys.* **11**, 033,021 (2009).
29. I. Marzoli, A. Kaplan, F. Saif, and W. Schleich, "Quantum carpets of a slightly relativistic particle," *Fortschr. Phys.* **56**(10) (2008).
30. M. Berry, I. Marzoli, and W. Schleich, "Quantum Carpets, Carpets of Light," *Phys. World* pp. 1–6 (2001).
31. M. Berry and S. Klein, "Integer, Fractional and Fractal Talbot Effects" *J. Mod. Opt.* **43**, 2139–2164 (1996).
32. J. F. Clauser, "Factoring Integers with Youngs N-Slit Interferometer," *Phys. Rev. A* **53**, 4587–4590 (1996).
33. S. Wölk, W. P. Schleich, "Quantum carpets: Factorization with degeneracies," *Proceedings of the Middleton Festival, Princeton*, in print (2009).
34. J. Yeazell and C. Stroud, "Observation of fractional revivals in the evolution of a Rydberg atomic wave packet," *Phys. Rev. A* **43**(9), 5153–5156 (1991).
35. M. Vrakking, D. Villeneuve, A. Stolow, "Observation of fractional revivals of a molecular wave packet," *Phys. Rev. A* **54**(1), 37 (1996).
36. J. H. Hannay, M. V. Berry, "Quantization of linear maps on a torus-fresnel diffraction by a periodic grating," *Physica* **1D** 267–290 (1980).

## 1. Self-imaging of periodic structures

In the early nineteenth century Talbot discovered the self-imaging of periodic structures through optical near-field diffraction [1]: When plane-parallel light falls onto an absorption mask with periodic openings the light will generate images of this grating in multiples of a well-defined distance, which is now called the Talbot length  $L_T$  (Figure 1).

Interferometric self-imaging is also possible for spatially incoherent light if we add a second grating down stream from the first one. It now suffices that the wave is fairly monochromatic but not necessarily collimated or transversally coherent. Lau identified the arrangements which generate distinct periodic images at various distances between the gratings and the observation screen [2]. These near-field fringe patterns that are based on a two-grating setup of Figure 2, are now commonly designated as Lau or Talbot-Lau images.

The theory of the optical Talbot effect was first developed by Rayleigh [3]. Meanwhile, a large number of theoretical treatments have discussed both the Talbot and the Talbot-Lau phenomena in great detail, with formalisms operating either in real space [4-8] or phase

space [9, 10]. Self-imaging of periodic transmission masks has attracted technological interest, as it allows to realize optical elements for waves that cannot be easily manipulated by standard refractive elements, such as lenses and prisms.

In light optics, the Talbot and Talbot-Lau effects were used for generating surface profiles of transparent objects [11, 12], for measuring the refraction of unknown materials or optical elements [13, 14], for recording temperature profiles in flames [15], for displacement sensors [16] or the sub-wavelength focusing of light [17].

Near-field diffraction at periodic structures has also been beneficial in plasmon [18] and x-ray physics [19, 20] and the near-field diffraction also bears fruits in the field of coherent matter-wave manipulation. The Talbot and Talbot-Lau effect for de Broglie waves were realized with atoms [21-25], large molecules [26, 27] and electrons [28]. They were even discussed for relativistic particles [29].

A recent review article by Berry, Marzoli and Schleich [30] pointed to the beauty of near-field diffraction and its many relations to other fields of mathematics and physics such as number factoring [31, 32, 33], the quantum particle in the box [31] or revivals of wave packets in Rydberg atoms [34] and molecules [35].

The authors of that review coined the terms *quantum carpets* and *carpets of light* to describe the densely woven and appealing interference structures that become apparent when the evolution of the wave intensity is traced as a function of the distance behind the grating. Although numerical simulations of the phenomenon were given [30] and even atomic carpets have been studied experimentally [23], it appears that full carpets of light have not been realized experimentally. The purpose of the present contribution is to close this gap.

## 2. The concept of optical carpets in the Talbot and Talbot-Lau arrangements

We start by giving a short derivation of the Talbot effect which reveals its conceptual simplicity and compares well with our optical experiments. We assume the grating at  $z = 0$  to span the  $x/y$  plane with its periodic modulation in the  $x$  direction. A plane wave falls onto the grating with the wave number  $k = 2\pi/\lambda$ . For the Talbot effect we will assume normal incidence but averaging over non-zero angles of incidence  $\theta$  (Figure 2a) will be required for the Talbot-Lau effect.

For static gratings we are allowed to factor out the time dependence of the field and the incident wave can be represented by  $\psi = e^{ik_\theta x}$  before it enters the grating. Here,  $k_\theta = k \sin(\theta)$  is the projection of the incident wave vector onto the  $x$ -axis.

The grating transforms the wave into

$$\psi(x, +0) = \psi(x, -0) \cdot T(x) = \sum_n A_n e^{i(k_\theta + nk_d)x} = \sum_n A_n e^{ik_{\perp,n}x} \quad (1)$$

where  $A_n$  represents the components of the Fourier decomposition of the periodic grating transmission function  $T(x)$ . We thus see that diffraction at a grating of period  $d$  simply adds multiples of  $k_d = 2\pi/d$  to the transverse wave vector of the incident plane wave.

When the wave function propagates a distance  $z$  from the grating to the screen it acquires an additional phase  $k_z z$  where  $k_{\perp,n}$  and  $k_z$  are the components of the wave vector perpendicular and parallel to the  $z$  axis, with  $k_z = [k^2 - k_{\perp,n}^2]^{1/2}$ . In the paraxial approximation ( $k_{\perp,n} \ll k$ ) we can expand the phase to second order into

$$\psi(x, z) = \sum_n A_n \exp \left[ i(k_\theta + nk_d)x + i \left( k - \frac{(k_\theta + nk_d)^2}{2k} \right) z \right]. \quad (2)$$

We now turn explicitly to the Talbot effect and set  $k_\theta = 0$  and obtain

$$\psi(x, z) = \sum_n A_n e^{ink_d x} e^{-in^2 \pi(z/L_T)}, \quad (3)$$

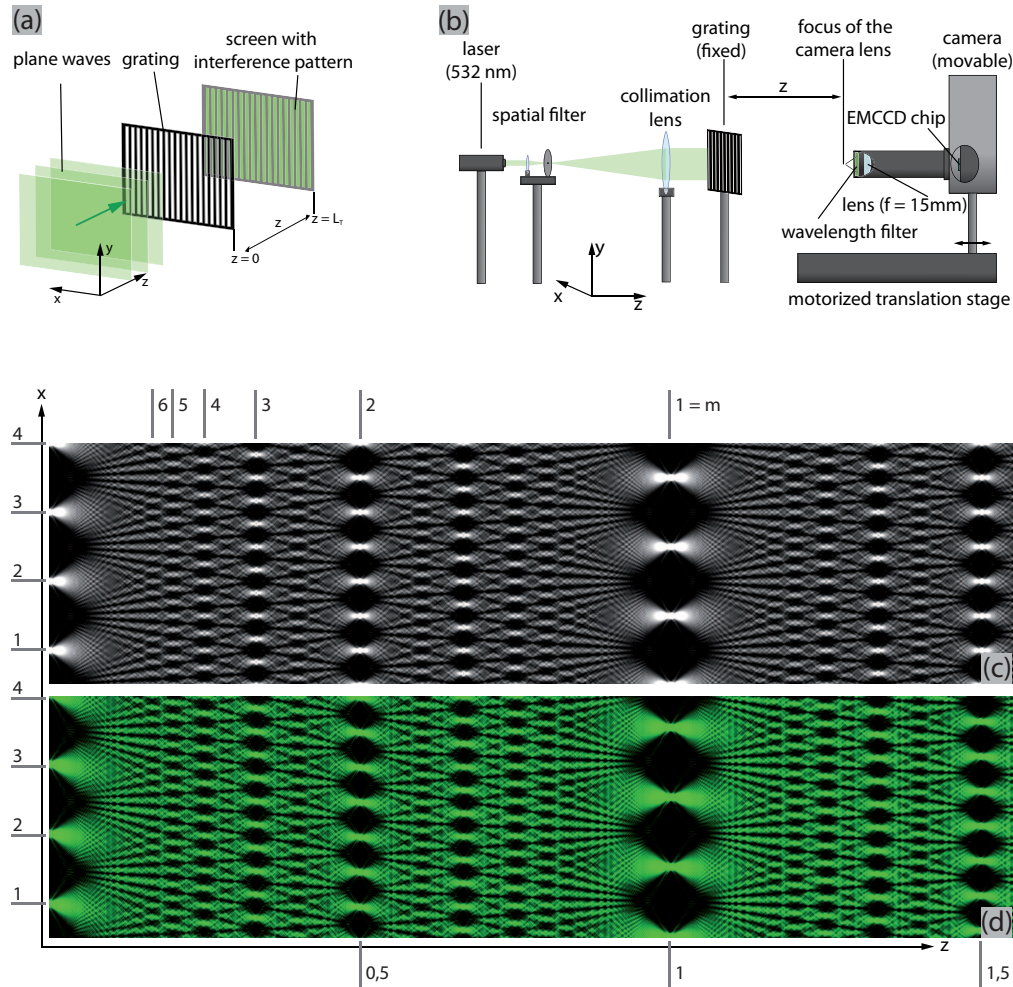


Fig. 1. (Color online) a) Talbot self-imaging using plane-parallel, monochromatic light waves; b) from left to right: laser at 532 nm, beam expander, grating, imaging lens in blackened lens tube and CCD detector on a micrometer translation stage; c) Theoretical expectation according to Eq. (3); d) Experimental carpet of light. The x-axis counts the grating periods. The z-axis represents the distance between the detector image plane and the grating in multiples of the corresponding Talbot distance. The numbers  $m$  indicate where self images of the  $m^{\text{th}}$  order are observed.

where an overall constant phase has been dropped and we have introduced the Talbot length  $L_T \equiv d^2/\lambda$ . The intensity pattern produced by the wave is obtained from  $I(x, z) = \psi(x, z)\psi^*(x, z)$ .

When the screen is at an even multiple of the Talbot length,  $z = 2n \cdot L_T$ , the wave pattern of Eq. (3) reproduces the transmitted amplitude at  $z = 0$  as described by Eq. (1). This interferometric self-imaging is the Talbot effect.

When  $z = L_T$  a similar simplification is possible. Since  $n$  odd implies  $n^2$  odd, and  $n$  even

implies  $n^2$  even it follows that  $e^{-in^2\pi} = e^{-in\pi}$  and Eq. (3) becomes

$$\psi(x, z = L_T) = \sum_n A_n e^{ink_d x} e^{-in\pi} = \sum_n A_n e^{ink_d(x-d/2)}. \quad (4)$$

In Eq. (4) we recover the original grating pattern but now displaced in  $x$  by half the grating constant. For infinitely extended gratings, this shifted self-image will again be repeated at all odd multiples of the Talbot length, i.e. for  $z = (2n + 1)L_T$ .

Interesting patterns also occur at a discrete set of other values of  $z$ . Consider the case when  $z$  can be represented as a rational multiple of the Talbot length,  $z = (s + p/r)2L_T$ , where  $s$ ,  $p$  and  $r$  are non-negative integers,  $p < r$  and  $p$  and  $r$  are relative primes. The  $z$  dependent factor in Eq. (3) becomes

$$e^{-in^2\pi(z/L_T)} = e^{-i2\pi n^2 p/r} \quad (5)$$

which is periodic in  $n$  with period  $r$ . We expand the expression in Eq. (5) in the discrete Fourier series

$$e^{-i\pi n^2 p/r} = \sum_{m=0}^{r-1} a_m e^{-i2\pi mn}. \quad (6)$$

The constants  $a_m$  can be found using Eq. (7)

$$\sum_{n=0}^{r-1} e^{-i2\pi mn/r} e^{i2\pi m' n/r} = r\delta_{mm'}. \quad (7)$$

For our expression Eq. (6) we find

$$a_m = \frac{1}{r} \sum_{n'=0}^{r-1} e^{-i2\pi(n'^2 - mn')p/r}, \quad (8)$$

and the field becomes

$$\begin{aligned} \psi(x, z) &= \sum_{m=0}^{r-1} a_m \sum_n A_n e^{-ink_d(x-md/r)} \\ &= \sum_{m=0}^{r-1} a_m \psi(x - md/r). \end{aligned} \quad (9)$$

The imaged field is a sum of shifted versions of the original grating pattern, each multiplied with a factor  $a_m$ . The expression for  $a_m$  given in Eq. (8) is a Gauss sum usually discussed in relation to number theory and its value depends on the relation between the integers  $p$ ,  $r$  and  $m$  [36]. For  $r$  odd all of the  $a_m$ 's are nonzero and have the same amplitude, independent of  $m$ . Thus for  $r$  odd the field represented in Eq. (10) is a superposition of  $r$  copies of the original field each of the same amplitude but with different phases. For  $r$  even ( $p$  odd) half of the  $a_m$ 's are zero while the other half are of the same nonzero amplitude but with different phases. For  $r$  even the field represented in Eq. (10) is a superposition of  $r/2$  copies of the original field each with the same amplitude but with different phases. Combining these cases we see that for  $z$  equal to an integer multiple of  $L_T$  the sum in Eq. (10) contains a single copy of the original wave. For  $z = L_T/2$  we get a superposition of two waves, for  $z = L_T/3$  or  $2L_T/3$  a superposition of three waves, and for  $z = L_T/4$  or  $3L_T/4$  four waves. Other rational fractions of  $L_T$  give similar results generating a very rich and detailed pattern [31]. If the grating has a small opening fraction  $f$ , i.e. if the width of the slits is much smaller than the grating period, these patterns will not overlap in lower orders ( $r$  small). In this case the resulting intensity pattern will be a sum of the shifted

grating transmission function. When the opening fraction is not sufficiently small the patterns will overlap and we expect them to be somewhat washed-out but still with considerable fine structure. As already shown by Berry and Klein [31] these carpets are true fractals and exhibit a very intricate pattern.

The grating multiplies the incoming wave alternately by one or zero, with an opening fraction of  $f = 0.1$  in our experiments. For such a grating the Fourier components are

$$\begin{aligned} A_0 &= f \\ A_n &= \sin(n\pi f)/(n\pi) \quad ; \text{for } n \neq 0 \end{aligned}$$

The resulting intensity distribution  $I = \psi \cdot \psi^*$  where  $\psi$  is taken from Eq. 3. It is reproduced using in Fig. 1c where the series has been truncated at  $n = \pm 25$ .

For the Talbot-Lau effect we now consider a spatially incoherent input beam. We simulate this by summing over all intensity distributions produced by waves that enter along a broad range of angles of incidence.

While the overlaying self-images would smear-out after a single grating, the addition of a second grating at  $z = L_1$  helps refocusing the waves to form again a clear grating image. This pattern can be viewed on a screen a distance  $L_2$  behind the second grating. The wave just before the second grating is given by Eq. (2) with  $z = L_1$ . If both gratings are identical the second one will impose the same periodic modulation as did the first, and the wave just after the second grating will be

$$\begin{aligned} \psi_\theta(x) &= \sum_{n,m} A_n A_m \exp[i(k_\theta + (n+m)k_d)x] \\ &\quad \times \exp[-i(k_\theta + nk_d)^2 L_1 / (2k)]. \end{aligned} \quad (10)$$

When propagated to the detection screen, Eq. (10) gives

$$\begin{aligned} \psi_\theta(x) &= \sum_{n,m} A_n A_m \exp[i(k_\theta + (n+m)k_d)x] \\ &\quad \times \exp[-i(k_\theta + nk_d)^2 L_1 / (2k)] \\ &\quad \times \exp[-i(k_\theta + (n+m)k_d)^2 L_2 / (2k)]. \end{aligned} \quad (11)$$

The squared modulus of Eq. (11) yields the final intensity pattern and reads

$$\begin{aligned} I_\theta = \psi_\theta \psi_\theta^* &= \sum_{n,m,n',m'} A_n A_m A_{n'}^* A_{m'}^* \exp[ik_d(n+m-n'-m')x] \cdot \\ &\quad \times \exp[-i2k_\theta k_d[(n-n')L_1 + (n-n'+m-m')L_2] / 2k] \\ &\quad \times \exp[-ik_d^2(n^2 - n'^2)L_1 / 2k] \exp[-ik_d^2((n+m)^2 - (n'+m')^2)L_2 / 2k]. \end{aligned} \quad (12)$$

In order to account for the spatially incoherent incident beam, we sum over all independent plane waves that originated from a variety of wave vector  $k_\theta$

$$I_{\text{Lau}} = \sum_{\theta} I_\theta. \quad (13)$$

Because of the  $k_\theta$ -dependence of Eq. (12) the pattern will be washed-out unless the coefficient of  $k_\theta$  is zero thus we require

$$L_2 = \frac{L_1}{\frac{m'-m}{n-n'} - 1}. \quad (14)$$

This imaging of various modes of the two gratings from an uncollimated beam is called the Talbot-Lau effect. Only terms in the Fourier expansion matching the condition given in Eq.(14)

will survive. Since higher order terms are expected to have small amplitudes  $A_n$ , the pattern will have a low visibility unless this condition holds among relatively small values of  $n, n', m, m'$ . Lau's original choice was  $m' - m = n - n'$  giving  $L_2 = \infty$ . Strong patterns can also be obtained with  $m' - m = 2(n - n')$  and  $L_2 = L_1$ . Both the Talbot and the Talbot-Lau effects can be implemented in a straight-forward way using elementary optical equipment.

### 3. Experimental realization of optical carpets

The Talbot experiment requires an approximately plane-parallel, monochromatic wave. We use the beam of a 5 mW green diode laser ( $\lambda = 532$  nm) which is expanded by an optical telescope to a diameter of 20 mm to cover the whole grating. A  $10 \mu\text{m}$  aperture in the focus of the beam expander acts as a spatial filter and mode cleaner to provide a homogeneous illumination. Since the final image covers only a transverse stretch of about one millimeter the Gaussian envelope of the laser beam intensity has negligible influence on the recorded pattern. The gratings are opaque for visible light (chromium on glass, Edmund Optics inc.), have a period of  $200 \mu\text{m}$  and an open fraction of 10%, i.e. an open slit width of  $20 \mu\text{m}$ .

Behind the grating, the Talbot fringes are recorded by an electron multiplying CCD camera (Andor Luca) with  $658 \times 496$  pixels of  $10 \mu\text{m}$  size. In order to see all details of wave interference, the Talbot images are magnified by a lens of short focal length ( $f_L = 15$  mm) which is mounted in a light-tight tube in front of the CCD-chip. Placed at a distance of 134 mm from the detector, the lens realizes a magnification factor of approximately nine. In order to further minimize stray light and reflections at the inner walls an iris is mounted in the middle of the lens-tube. A laser line filter ( $\lambda_0 = 532$  nm,  $\Delta\lambda_{1/2} = 10 \pm 2$  nm) effectively reduces the influence of external stray light. A motorized translation stage allows to shift the detector with micrometer resolution for more than 100 mm along the z-axis.

We then follow the optical interference along the beam path by shifting the camera in steps of  $\Delta z = 50 \mu\text{m}$  and taking a CCD snapshot in each position. Care has to be taken to ensure a good alignment between the axis of the translation stage and the k-vector to the incident laser beam: their relative angle must be smaller than 1 mrad to avoid a transverse shift of the detected interference pattern when the staged is moved.

Since the grating is a perfectly periodic structure we can average over the vertical pixels to improve signal-to-noise ratio, provided that the lines in both the grating and the CCD array have been sufficiently well aligned. For each longitudinal position (z) the two-dimensional patterns  $I(x, y; z)$  are transformed into one-dimensional horizontal traces  $I(x; z) = \sum_y I(x, y; z)$  which we then merge for all z-positions into a single Talbot-carpet  $I(x, z)$ .

The result of this procedure is shown in Figure 1d which fits in great detail to the theoretical expectation of Figure 1c. Generally, the amount of fine details in the model increases with the number of summands. For Figure 1c the sum could be truncated at  $n = \pm 25$  and still reproduces the experiment with high accuracy down to the finest details.

At integer multiples of the Talbot length  $L_T = d^2/\lambda = 75.2$  mm we identify the grating's self-image. Rescaled patterns can be found in rational fractions of  $L_T$ , as indicated by the tic-marks in Figure 1c/d.

In order to realize the Talbot-Lau experiment we insert a second grating between the first grating and the light source. This second diffraction structure is identical to the first one and is mounted on a translation stage. Both the distance  $L_1$  between the gratings as well as the distance  $L_2$  between  $G_2$  and the image plane can be scanned. Similarly to the Talbot arrangement, we have to align the axes of both translation stages and the laser beam to be parallel within 1 mrad. We now use a low-pressure sodium lamp in combination with a frosted glass plate as a spatially incoherent but rather monochromatic light source. The sodium lamp dominantly emits at 589.3 nm. The atomic hyperfine structure cannot be resolved in this experiment.

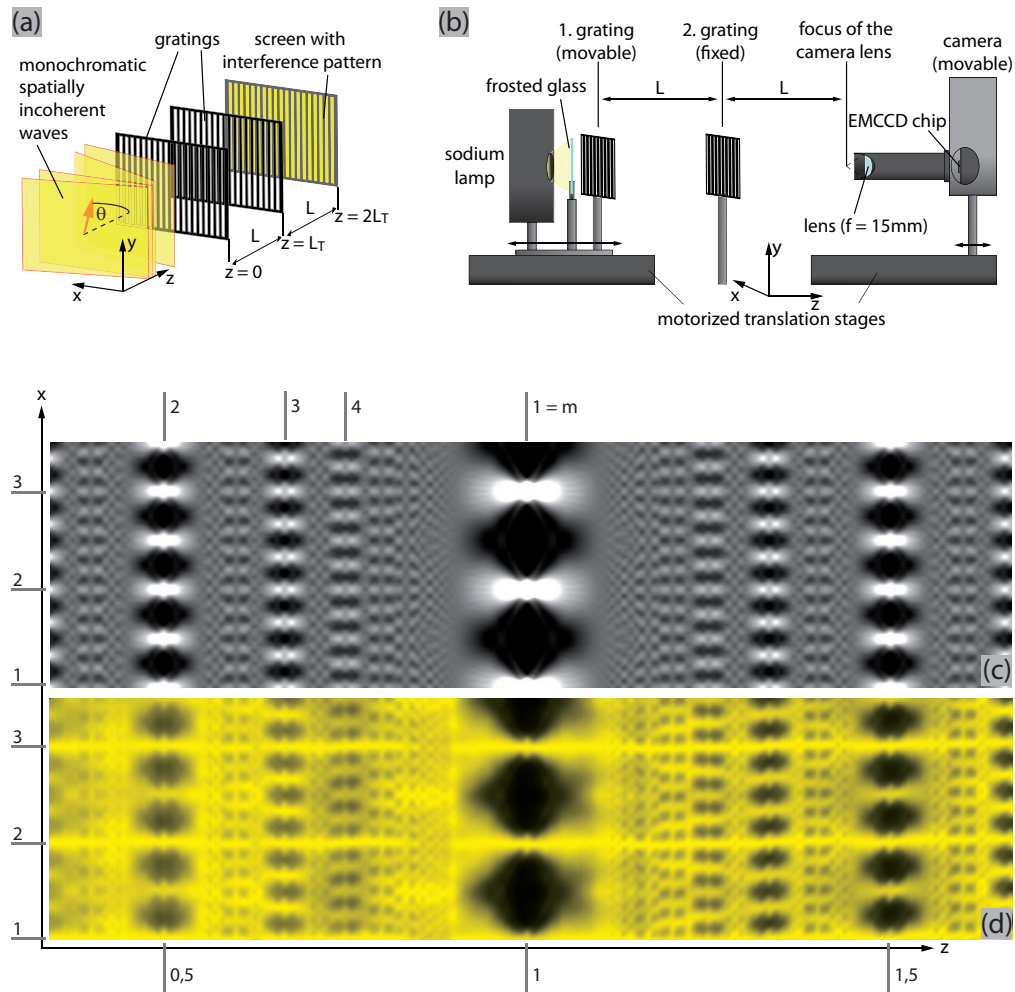


Fig. 2. (Color online) a) Talbot-Lau imaging with spatially incoherent light: A monochromatic but spatially incoherent beam of light can be decomposed into a bundle of plane waves covering a range of incident angles. Since the laterally shifted self-images overlap non-synchronously they wash out. Insertion of a second grating leads to the refocusing of the diverging wavefronts and to the emergence of a Talbot-Lau interference pattern. b) Experimental implementation with a filtered sodium lamp. The frosted glass transforms the incident light into a diffusely scattered, spatially incoherent beam. The first grating prepares spatial coherence, the second grating rephases the outgoing waves which then interfere in the image plane of the camera lens; c) Computational simulation according to Eq. (13); d) Experimental Talbot-Lau carpet. The  $z$ -axis now represents the distance  $L_1$  between the gratings  $G_1$  and  $G_2$  which equals the distance between  $G_2$  and the imaging plane; The numbers  $m$  indicate where self images of the  $m^{\text{th}}$  order are observed.

We first balance  $L_1$  and  $L_2$  by optimizing the sharpness of the interference pattern on the CCD chip. For  $d = 200 \mu\text{m}$  and  $\lambda = 589 \text{ nm}$  the Talbot length amounts to 67.9 mm. Both the camera and the grating are then scanned in steps  $\Delta z = 50 \mu\text{m}$  to keep the distances balanced.

The result of that experiment is shown in Figure 2d which is well reproduced by the theoretical model of Figure 2c with  $n = \pm 20$ . Again we find an intricate fine structure, including rational fractions of the Talbot image. Little differences between theory and experiment derive from the infrared and UV lines emitted by the sodium lamp. The additional stripes that show up in the experiment without being reproduced in the simulation are attributed to spurious wavelengths in the UV and IR. The sodium lamp emits dominantly in the yellow spectral range (589 nm, 90% of total intensity). Additional wavelengths create carpets of similar transverse structure but with a different longitudinal scaling behavior. The second-most intense wavelength can be found at 819 nm. It produces a carpet with  $L_T = 48.8 \text{ mm}$ . The grating self-image in the IR can be seen as an additional feature at  $3/4$  of the yellow Talbot length.

The present work thus nicely illustrates advanced wave optics in the Talbot and Lau configuration. Intuitive demonstrators of the kind presented here are easily realized in any optics lab and they help to derive new ideas for more complex investigations with ultra-sound, x-rays, electrons, atoms and molecules.

### Acknowledgments

We would like to thank Wolfgang Schleich for stimulating discussions. This work has been supported by the FWF within the project Z149-N16. SD acknowledges an ÖAD travel grant and support by the National Electronics and Computer Technology Center, National Science and Technology Development Agency and Industry/University Cooperative Research Center (IUCRC) in HDD Component, the Faculty of Engineering, Khon Kaen University.